SIAM J. IMAGING SCIENCES
Vol. 1, No. 4, pp. 364–378

Convex Source Support and Its Application to Electric Impedance Tomography*

Martin Hanke†, Nuutti Hyvönen‡, and Stefanie Reusswig†

Abstract. The aim in electric impedance tomography is to recover the conductivity inside a physical body from boundary measurements of current and voltage. In many situations of practical importance, the investigated object has known background conductivity but is contaminated by inhomogeneities. In this work, we try to extract all possible information about the support of such inclusions inside a two-dimensional object from only one pair of measurements of impedance tomography. Our noniterative and computationally cheap method is based on the concept of the convex source support, which stems from earlier works of Kusiak, Sylvester, and the authors. The functionality of our algorithm is demonstrated by various numerical experiments.

Key words. electric impedance tomography, inverse source problems, scattering support, source support, inclusions

AMS subject classifications. 35R30, 65N21

DOI. 10.1137/080715640

1. Introduction.

Let us consider the inverse boundary value problem of *electric impedance tomography* (EIT) in a bounded simply connected domain $D \subset \mathbb{R}^2$: Determine the conductivity $\sigma : D \to \mathbb{R}$, with $0 < \underline{\sigma} \le \sigma(x) \le \overline{\sigma} < \infty$, in the elliptic equation

$$\nabla \cdot (\sigma \nabla v) = 0 \quad \text{in } D, \qquad \sigma \frac{\partial v}{\partial \nu} = f \quad \text{on } \partial D, \qquad \int_{\partial D} v \, \mathrm{d}s = 0 \tag{1.1}$$

using all possible boundary measurement pairs $(v|_{\partial D}, f)$. Here, v is the electrostatic potential, and f is the mean free boundary current inserted into the body. Astala and Päivärinta [1] have shown that this problem is uniquely solvable for a general isotropic conductivity; see also [2, 3, 23, 27]. However, due to the severe ill-posedness of the problem, there is little hope of building a reliable algorithm for reconstructing general conductivities. In particular, this is true if only a few Cauchy data pairs $(v|_{\partial D}, f)$ are available, which in practice is often the case.

In this work we are interested in a more specific application of EIT. Various imaging problems of practical importance consider locating inhomogeneities inside objects with known background conductivities. For example, detection of cracks and air bubbles in some building material and distinguishing cancerous tissue from healthy background fall into this category

*Received by the editors February 14, 2008; accepted for publication (in revised form) July 23, 2008; published electronically December 3, 2008.
http://www.siam.org/journals/siims/1-4/71564.html
†Institut für Mathematik, Johannes Gutenberg-Universität Mainz, 55099 Mainz, Germany (hanke@math.uni-mainz.de, reusswig@math.uni-mainz.de). The work of the third author was supported by the Deutsche Forschungsgemeinschaft (DFG) under grant HA2121/6-1.
‡Institute of Mathematics, Helsinki University of Technology, FI-02015 HUT, Finland (nuutti.hyvonen@hut.fi). The work of this author was supported by the Academy of Finland (project 115013), the Finnish Cultural Foundation, the Finnish Foundation for Technology Promotion, and the Finnish Funding Agency for Technology and Innovation (project 40084/06).

of problems. If the background conductivity is assumed to be constant, say 1, our problem setting can be expressed as follows: Assuming that

$$\sigma - 1 \quad \text{has compact support within } D,$$

i.e., σ is 1 near the boundary of D, gather information on $\operatorname{supp}(\sigma - 1)$ from only one (or a few) Dirichlet–Neumann pair of boundary data for problem (1.1).

Generating the corresponding harmonic reference potential v_0, i.e., the solution of (1.1) with σ replaced by 1, we can reduce our problem to finding the support of the source in the Poisson equation

$$\Delta u = F \quad \text{in } D, \qquad \frac{\partial u}{\partial \nu} = 0 \quad \text{on } \partial D, \qquad \int_{\partial D} u \, \mathrm{d}s = 0, \tag{1.2}$$

where $u = v - v_0$ and the source can be written formally as

$$F \;=\; \nabla \cdot (1 - \sigma) \nabla v \,.$$

Note that this notation has to be properly interpreted in a distributional sense if σ lacks the appropriate smoothness (cf. section 4), but nonetheless, F is always supported within the support of $\sigma - 1$. Also note that each pair of Dirichlet–Neumann data for problem (1.1) leads to a different source, and thus, in principle, to additional information about the support of $\sigma - 1$.

In a series of papers [7, 19, 20, 24, 25, 26], Kusiak and Sylvester, with varying coauthors, developed the concept of convex scattering support, which is meant to be the smallest convex set that contains a scattering source compatible with the far field of a scattered wave. The corresponding theory was presented in [10] for electrostatics, and the notion of convex source support was introduced. The purpose of the present paper is to develop an efficient algorithm for computing the convex source support corresponding to the measurement $u|_{\partial D} = (v - v_0)|_{\partial D}$ in (1.2) and thus introduce a method for extracting information on the location of the support of the inhomogeneity $\sigma - 1$ from only one (or a few) measurement of EIT.

The outline of our paper is as follows. In section 2 we introduce the concept of convex source support and study some of its basic properties. Section 3 develops a constructive way to locate the convex source support, and section 4 builds an efficient numerical algorithm for detecting inclusions using only one measurement of EIT. The functionality of the algorithm is then demonstrated in section 5 by numerical examples.

2. The convex source support.

Assume that $D \subset \mathbb{R}^2$ is a bounded and simply connected domain with a smooth enough, say C^2, boundary. As noted in [10], the problem (1.2) has a well-defined and unique solution $u \in \cup_{m \in \mathbb{Z}} H^m(D)$ for any distributional source F in

$$\mathcal{E}'_\diamond(D) = \left\{ v \in \mathcal{E}'(D) \mid \langle v, 1 \rangle = 0 \right\},$$

where $\langle \cdot, \cdot \rangle : \mathcal{E}'(D) \times C^\infty(D) \to \mathbb{C}$ denotes the dual evaluation between compactly supported distributions and smooth functions in D. Moreover, the solution u is smooth in some neighborhood of the boundary ∂D. In consequence, the following linear operator is well defined:

$$L : \begin{cases} F \mapsto u|_{\partial D}, \\ \mathcal{E}'_\diamond(D) \to L^2_\diamond(\partial D), \end{cases}$$

where $L^2_\diamond(\partial D)$ denotes the space of square integrable mean free functions on ∂D. We denote the range and the null space of L by $\mathcal{R}(L)$ and $\mathcal{N}(L)$, respectively.

It is easy to see that L is not injective and not even the support of F is uniquely determined by the boundary measurement $g = LF$ (cf. [10, 19]). Furthermore, the intersection of the supports of the sources compatible with g is, in general, empty (cf. [19]), and this may hold even if the holes in the supports are included before the intersection is taken [10]. However, intersecting the convex hulls of the supports of the compatible sources provides information on the original source as explained in the following (cf. [10]).

The *convex support* $\operatorname{supp}_c F$ of $F \in \mathcal{E}'_\diamond(D)$ is the convex hull of the support $\operatorname{supp} F$ of F. Furthermore, the *convex source support* $\mathcal{C}g$ is given by

$$\mathcal{C}g = \bigcap_{LF=g} \operatorname{supp}_c F \tag{2.1}$$

if $g \in \mathcal{R}(L)$, and $\mathcal{C}g$ is defined to be the convex hull of D, $\operatorname{ch} D$, otherwise. Take note that if D is nonconvex, $\mathcal{C}g$ is not necessarily a subset of D.

It can been shown that $\mathcal{C}g$ is essentially the smallest convex set that carries a source that is compatible with g; the following theorem is a restatement of [10, Theorem 4.1] without the assumption that D is convex. Here and in what follows, $N_\epsilon(\Omega)$ denotes the open epsilon neighborhood of a set $\Omega \subset \mathbb{R}^2$; i.e.,

$$N_\epsilon(\Omega) = \{x \in \mathbb{R}^2 \mid \operatorname{dist}(x, \Omega) < \epsilon\},$$

where $\operatorname{dist}(x, \Omega) = \inf_{y\in\Omega} |x - y|$. The closure of Ω is denoted by $\overline{\Omega}$.

Theorem 2.1. *Let $g \in \mathcal{R}(L)$. Then, given any $\epsilon > 0$, there exists a source $F_\epsilon \in \mathcal{E}'_\diamond(D)$ such that $LF_\epsilon = g$ and*

$$\mathcal{C}g \subset \operatorname{supp}_c F_\epsilon \subset \overline{N_\epsilon(\mathcal{C}g)}.$$

Moreover, $\mathcal{C}g = \emptyset$ if and only if $g = 0$.

Proof. Assume first that $\mathcal{C}g \neq \emptyset$ and fix an arbitrary $\epsilon > 0$ such that $N_\epsilon(\mathcal{C}g) \subset \operatorname{ch} D$. It follows from a compactness argument (cf. [19]) that we can find a finite number $F_1, \ldots, F_n$ of compatible sources such that

$$C := \bigcap_{k=1}^{n} \operatorname{supp}_c F_k \subset N_\epsilon(\mathcal{C}g).$$

For each $k = 1, \ldots, n$ there exists a harmonic function u_k in $D \setminus \operatorname{supp} F_k$ with the Cauchy data $(g, 0)$ on ∂D. Since $\operatorname{supp}_c F_k$ and $\operatorname{supp}_c F_j$ are convex sets, u_k and u_j coincide in $D \setminus (\operatorname{supp}_c F_k \cup \operatorname{supp}_c F_j)$, and all of these functions can be extended (or restricted) as the same harmonic function u to $D \setminus C \supset D \setminus N_\epsilon(\mathcal{C}g)$. Furthermore, due to the principle of unique continuation, all u_k agree in $N_\delta(\partial D) \cap D$ for some $\delta > 0$ that depends on the chosen sources. Hence, we can continue u harmonically to the whole of $(D \setminus C) \cup (N_\delta(\partial D) \cap D)$ with the Cauchy data $(g, 0)$ on ∂D. By taking $F_\epsilon = \Delta u_\epsilon$, with $u_\epsilon \in L^2(D)$ defined as

$$u_\epsilon = \begin{cases} u & \text{in } (D \setminus N_\epsilon(\mathcal{C}g)) \cup (N_{\delta/2}(\partial D) \cap D), \\ 0 & \text{otherwise,} \end{cases}$$

we have thus constructed an appropriate source.

If $g = 0$, then the trivial source $F_\epsilon = 0$ is compatible with the data and, in particular, $\mathcal{C}g = \operatorname{supp}_c F_\epsilon = \emptyset$. On the other hand, if $\mathcal{C}g = \emptyset$, then a compactness argument reveals that there exist a finite number of compatible sources and associated convex supports such that the intersection C of these convex sets is empty. As above, the corresponding harmonic potentials can be continued to a univalent harmonic function u that solves the Cauchy problem for the data $(g, 0)$ in $D \setminus C = D$. As u has homogeneous Neumann boundary value, it must be constant in D, and hence its trace g must vanish as it is mean free. This completes the proof. ∎

2.1. Extension to a disk. In the following sections we will build a cheap numerical algorithm for reconstructing the convex source support in the case that the domain of interest is a disk. To show that considering this special case is sufficient from the practical point of view, let us explain how the measurement g on ∂D, corresponding to a source in D, provides a stable way to construct the measurement corresponding to problem (1.2) with the very same source F, but posed in an origin-centered disk $B_\rho \supset \overline{D}$ of radius ρ instead of D. At the same time, we will examine whether the convex source support is affected by this extension process.

Let us consider the transmission problem

$$\begin{aligned} &\Delta w = 0 \quad \text{in } B_\rho \setminus \partial D, \qquad \frac{\partial w}{\partial \nu} = 0 \quad \text{on } \partial B_\rho, \qquad \int_{\partial B_\rho} w \, \mathrm{d}s = 0, \\ &\frac{\partial w^+}{\partial \nu} - \frac{\partial w^-}{\partial \nu} = 0, \qquad w^+ - w^- = g \quad \text{on } \partial D, \end{aligned} \tag{2.2}$$

where $g = u|_{\partial D}$ for the solution of (1.2) and the superscripts $+$ and $-$ correspond to traces taken from within $B_\rho \setminus \overline{D}$ and D, respectively. The problem (2.2) has a unique solution w_ρ in $H^1(D) \oplus H^1(B_\rho \setminus \overline{D})$, i.e., among $L^2(B_\rho)$-functions that are in H^1 when restricted to D or to $B_\rho \setminus \overline{D}$. We denote the zero continuation of u to the whole of B_ρ by u_0, set $u_\rho = u_0 + w_\rho$, and note that $\mathcal{E}'_\diamond(D)$ can be considered as a subspace of $\mathcal{E}'_\diamond(B_\rho)$ via extension by zero (cf. [6]).

Lemma 2.2. *The distribution $u_\rho \in \cup_{m\in\mathbb{Z}} H^m(B_\rho)$ is the unique solution of the Poisson problem*

$$\Delta u = F \quad \text{in } B_\rho, \qquad \frac{\partial u}{\partial \nu} = 0 \quad \text{on } \partial B_\rho, \qquad \int_{\partial B_\rho} u \, \mathrm{d}s = 0. \tag{2.3}$$

Proof. Since the Dirichlet and Neumann boundary values of u_ρ are continuous over ∂D and the Laplacians of both u_0 and w_ρ vanish away from the set $\partial D \cup \operatorname{supp} F$, it follows that

$$\Delta u_\rho = F \quad \text{in } B_\rho.$$

Hence, the claim is a consequence of the outer boundary conditions of (2.2). ∎

Notice that (2.2) can be solved in a stable manner. Hence, given the data $g \in L^2_\diamond(\partial D)$ corresponding to (1.2) with a source $F \in \mathcal{E}'_\diamond(D)$, Lemma 2.2 provides the means to compute the "propagated" data $g_\rho \in L^2_\diamond(\partial B_\rho)$ corresponding to (2.3) and the very same source. Next we will examine what happens to the convex source support when the domain is expanded in this way.

Let L_ρ be the operator that maps a source $F \in \mathcal{E}'_\diamond(B_\rho)$ onto the Dirichlet boundary value of the solution to (2.3) $u_\rho|_{\partial B_\rho} \in L^2_\diamond(\partial B_\rho)$. The following lemma provides a relation between the convex source supports corresponding to a fixed source and the domains D and B_ρ, respectively. Notice that the convex source support $\mathcal{C}_\rho g_\rho$ of the data $g_\rho \in L^2_\diamond(\partial B_\rho)$ is defined in accordance with (2.1); i.e.,

$$\mathcal{C}_\rho g_\rho = \bigcap_{L_\rho F = g_\rho} \operatorname{supp}_c F \tag{2.4}$$

if $g_\rho \in \mathcal{R}(L_\rho)$, and $\mathcal{C}_\rho g_\rho = B_\rho$ otherwise. Bear in mind that in (2.4) the sources live in $\mathcal{E}'_\diamond(B_\rho)$, which is a larger space than $\mathcal{E}'_\diamond(D)$.

Theorem 2.3. *The sets $\mathcal{N}(L)$ and $\mathcal{N}(L_\rho) \cap \mathcal{E}'_\diamond(D)$ coincide. In particular, if $g = LF$ and $g_\rho = L_\rho F$ for some $F \in \mathcal{E}'_\diamond(D)$, then $\mathcal{C}_\rho g_\rho \subset \mathcal{C} g$, where equality holds if D is convex.*

Proof. If $LF = 0$ for some $F \in \mathcal{E}'_\diamond(D)$, it follows immediately from Lemma 2.2 and the unique solvability of (2.2) that also $L_\rho F = 0$. Assume next that $L_\rho F = 0$ for some mean free distribution F supported inside D. The corresponding potential u_ρ of (2.3) vanishes in $N_\epsilon(B_\rho \setminus D) \cap B_\rho$ for some $\epsilon > 0$ due to the unique solvability of the Cauchy problem on ∂B_ρ. This implies that $u_\rho|_{\partial D}$ and the flux of u_ρ across ∂D are both zero, and, hence, $u_\rho|_D$ solves the source problem (1.2). In particular, $LF = u_\rho|_{\partial D} = 0$, which completes the first part of the proof.

Next, let $g = LF$ and $g_\rho = L_\rho F$ for $F \in \mathcal{E}'_\diamond(D)$. If $g = L\tilde{F}$ for some other $\tilde{F} \in \mathcal{E}'_\diamond(D)$, the first part of the theorem tells us that also $g_\rho = L_\rho \tilde{F}$. Hence, $\mathcal{C}_\rho g_\rho \subset \mathcal{C} g$. Let us then make the additional assumption that D is convex. Due to Theorem 2.1, there exists a source $F_\epsilon \subset \mathcal{E}'_\diamond(B_\rho)$ such that for a small enough $\epsilon > 0$

$$L_\rho F_\epsilon = g_\rho, \qquad \operatorname{supp}_c F_\epsilon \subset \overline{N_\epsilon(\mathcal{C}_\rho g_\rho)} \subset \overline{N_\epsilon(\mathcal{C} g)} \subset D,$$

where the last inclusion is a consequence of the convexity of D. Hence, it follows from the first part of the theorem that $LF_\epsilon = g$. In particular, $\mathcal{C} g$ belongs to $\overline{N_\epsilon(\mathcal{C}_\rho g_\rho)}$ for every $\epsilon > 0$, which implies that $\mathcal{C} g \subset \mathcal{C}_\rho g_\rho$. ∎

Notice that in general the sets $\mathcal{C} g$ and $\mathcal{C}_\rho g_\rho$ of Theorem 2.3 do not coincide if D is nonconvex, as the following example demonstrates. In other words, the convex source support does not depend merely on the source generating the data but also on the nonconvex domain where it lives; for all convex domains the convex source support is the same, however.

Example 1. Consider the auxiliary function $u_1(x) = \arg(x - (1/2, 0)) - \arg(x + (1/2, 0))$ in the disk B_ρ, $\rho = 1$; here the function arg returns the polar angle $\theta \in (-\pi, \pi]$ of its argument. A simple symmetry argument reveals that the Neumann boundary value of u_1 has vanishing mean, which implies that the source $F_1 = \Delta u_1$, supported on the closed line segment $\Gamma_1 := [(-1/2, 0), (1/2, 0)]$, belongs to $\mathcal{E}'_\diamond(B_\rho)$. When restricted to the lower half-plane, u_1 can be continued harmonically across the open line segment corresponding to Γ_1, making it possible to define a second auxiliary function u_2 that is harmonic in the complement of the dashed curve Γ_2 depicted in the left-hand image of Figure 1 and agrees with u_1 in the complement of the closed D-shaped region bounded by Γ_1 and Γ_2. In particular, u_1 and u_2 jump by 2π when crossing Γ_1 and Γ_2, respectively. We define a second source, supported on Γ_2, by $F_2 = \Delta u_2$. Since the Neumann boundary values of u_1 and u_2 can be made homogeneous

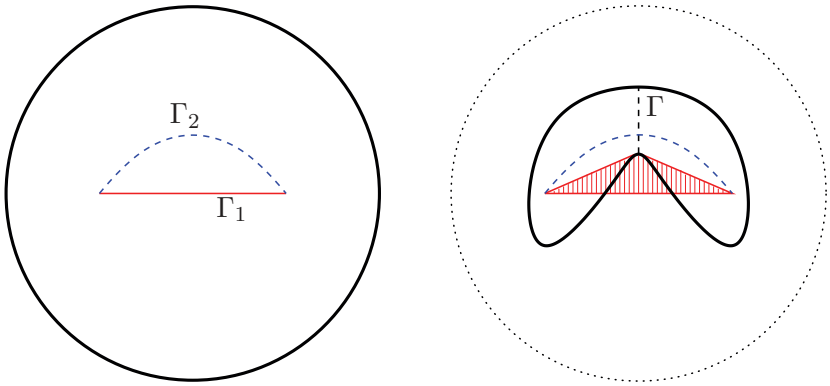

Figure 1. *Geometry of Example 1 (see text). Left: The supports of two equivalent sources in a disk; the lower one coincides with the corresponding convex source support. Right: The upper source in a kite-shaped domain; the corresponding convex source support is the closed region filled with vertical lines.*

by subtracting the same harmonic function, it follows easily that $L_\rho F_1 = L_\rho F_2 =: g_\rho$. As in Example 3.3 of [10], we may argue that every source compatible with the data g_ρ must contain both $(-1/2, 0)$ and $(1/2, 0)$ in its convex support, meaning that $\mathcal{C}_\rho g_\rho = \Gamma_1$. (Take note that Γ_2 could have been chosen as any smooth curve that is contained in the intersection of B_ρ and the upper half-plane, does not intersect itself, and has the end points $(-1/2, 0)$ and $(1/2, 0)$.)

Consider then the above defined source $F_2 \in \mathcal{E}'_\diamond(D)$ in the kite-shaped domain D marked by the thick solid curve in the right-hand image of Figure 1; it is important that D is chosen so that Γ_2 is its subset, but Γ_1 is not. Since the solution of (1.2) corresponding to F_2, say $\tilde{u}_2$, differs from $u_2|_D$ by a harmonic function that has the same Neumann boundary value as u_2 on ∂D, it follows that $\tilde{u}_2$ also jumps by 2π when crossing the curve Γ_2. In particular, $\tilde{u}_2$ is discontinuous in any neighborhood of $(-1/2, 0)$, or in that of $(1/2, 0)$, and it follows easily from the principle of unique continuation that the Cauchy data $(LF_2, 0)$ cannot be continued harmonically to any neighborhood of either of these two points. As a consequence, every $\mathcal{E}'_\diamond(D)$-source that is compatible with the data $g := LF_2$ must contain both $(-1/2, 0)$ and $(1/2, 0)$ in its convex support.

Let Γ be the dashed vertical line segment depicted in Figure 1; it is important that Γ divides D into two connected components and that $(-1/2, 0)$ and $(1/2, 0)$ are on different sides of Γ. Every compact subset of D that supports a source that is compatible with the data g must intersect Γ. Otherwise, due to the principle of unique continuation, there would exist $\epsilon > 0$ and a harmonic function in $N_\epsilon(\partial D \cup \Gamma) \cap D$ that would coincide with $\tilde{u}_2$ in $(N_\epsilon(\partial D \cup \Gamma) \cap D) \setminus \Gamma_2$, which contradicts the jump condition of $\tilde{u}_2$ on Γ_2. To sum up, any source that is compatible with g must contain the points $(-1/2, 0)$ and $(1/2, 0)$ and some part of Γ in its convex support, and so it follows from the definition (2.1) that $\mathcal{C}g \neq \Gamma_1$. This shows that the convex source supports corresponding to the measurements LF_2 and $L_\rho F_2$ do not coincide. (By letting the curve Γ_2 approach the bottom edge of D from above, one can actually argue that $\mathcal{C}g$ is the closed, almost triangular, region filled by vertical lines in the right-hand image of Figure 1.) This completes the example.

To sum up, if D is convex, the convex source support is not affected by extending the source

problem to a disk containing the original domain D. On the other hand, if D is nonconvex, this procedure can make the convex source support smaller. However, in all cases the new convex source support is still a nonempty subset of the convex hull of the unknown source generating the original measurement, and thus it contains quite a bit of useful information.

If we confine ourselves to looking for the convex source support corresponding to the original source generating the data and any convex domain enclosing the original domain, up to solving one elliptic boundary value problem of the type (2.2), we may assume that our two-dimensional domain of interest is a disk to begin with. After appropriate scaling, this disk can be considered to be the unit disk. This is the convention we will adopt in the rest of this work.

3. Constructive approximation of the convex source support. From now on, we will assume that D is the unit disk. In this section we will build a criterion for deciding if the convex source support $\mathcal{C}g$ lies in the intersection of D and a given closed disk $B \subset \mathbb{R}^2$. Since the closed disks enclosing a closed and convex set define that set uniquely, this gives us a tool for reconstructing $\mathcal{C}g$.

Let $F \in \mathcal{E}'_\diamond(D) \subset \mathcal{E}'_\diamond(B_\rho)$, $\rho \geq 1$, be a fixed but unknown source and consider both $g = LF$ and $g_\rho = L_\rho F$ as functions of the polar angle θ. We denote the Fourier coefficients of g and g_ρ by $\{\alpha_j\}_{j=-\infty}^{\infty}$ and $\{\beta_j\}_{j=-\infty}^{\infty}$, respectively, i.e.,

$$\alpha_j = \frac{1}{2\pi}\int_{-\pi}^{\pi} g(\theta)e^{-\mathrm{i}j\theta}\,\mathrm{d}\theta, \qquad \beta_j = \frac{1}{2\pi}\int_{-\pi}^{\pi} g_\rho(\theta)e^{-\mathrm{i}j\theta}\,\mathrm{d}\theta, \qquad j \in \mathbb{Z}.$$

The following lemma provides a simple relation between the above sets of Fourier coefficients.

Lemma 3.1. *The Fourier coefficients of g and g_ρ are related through*

$$\beta_j = \frac{\alpha_j}{\rho^{|j|}}, \qquad j \in \mathbb{Z}. \tag{3.1}$$

Proof. It is easy to see that in our concentric framework the solution of (2.2) can be given in polar coordinates as

$$w_\rho(r,\theta) = \begin{cases} \frac{1}{2}\displaystyle\sum_{j=-\infty}^{\infty} \alpha_j \left(\rho^{-2|j|} - 1\right) r^{|j|} e^{\mathrm{i}j\theta}, & (r,\theta) \in (0,1) \times (-\pi,\pi], \\ \frac{1}{2}\displaystyle\sum_{j=-\infty}^{\infty} \alpha_j \left(\rho^{-2|j|} r^{|j|} + r^{-|j|}\right) e^{\mathrm{i}j\theta}, & (r,\theta) \in (1,\rho) \times (-\pi,\pi]. \end{cases}$$

In particular, according to Lemma 2.2, we have

$$g_\rho(\theta) = (w_\rho|_{\partial B_\rho})(\theta) = \sum_{j=-\infty}^{\infty} \frac{\alpha_j}{\rho^{|j|}} e^{\mathrm{i}j\theta},$$

which proves the claim. ∎

Given a general closed disk $B \subset \mathbb{R}^2$ and B_ρ, with a large enough radius $\rho \geq 1$, containing B, there is a conformal map, more precisely, a Möbius transformation $\Phi : B_\rho \to D$, that maps

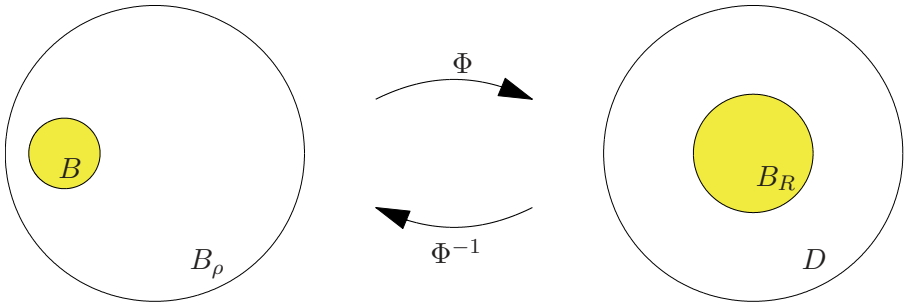

Figure 2. *The conformal mapping.*

$\overline{B}_\rho$ onto $\overline{D}$ and B onto some disk $\overline{B}_R \subset D$ centered at the origin (cf. Figure 2); the radius $R = R(B,\rho)$ of $\overline{B}_R$ is uniquely determined by B and ρ (cf., e.g., Henrici [11]). We denote the Fourier coefficients of $g_\rho \circ \Phi^{-1}$ by $\{\alpha_j(\Phi)\}_{j=-\infty}^{\infty}$. Notice that they can be computed efficiently from the mere knowledge of g and Φ by using the representation given in Lemma 3.1.

Theorem 3.2. *The function $g_\rho \in L^2_\diamond(\partial B_\rho)$ can be written as $g_\rho = L_\rho \tilde{F}$ for some $\tilde{F} \in \mathcal{E}'_\diamond(B_\rho)$ with* $\operatorname{supp} \tilde{F} \subset B$ *if and only if there exists $m \in \mathbb{Z}$ such that*

$$\sum_{j=-\infty}^{\infty} \frac{|\alpha_j(\Phi)|^2}{R(B,\rho)^{2|j|}} \langle j \rangle^m < \infty,$$

where we have used the notation $\langle j \rangle = (1+j^2)^{1/2}$.

Proof. The claim follows by using the exact same reasoning as in the proof of [10, Lemma 5.3]. ∎

Corollary 3.3. *Let $g \in \mathcal{R}(L)$. Then we have $\mathcal{C}g = \mathcal{C}_\rho g_\rho \subset B \cap D$ if and only if*

$$\sum_{j=-\infty}^{\infty} \frac{|\alpha_j(\Phi)|^2}{(R+\epsilon)^{2|j|}} < \infty \tag{3.2}$$

for $R = R(B,\rho)$ and every $\epsilon > 0$.

Proof. In our concentric framework, the relation $\mathcal{C}g = \mathcal{C}_\rho g_\rho$ is a consequence of Theorem 2.3. Moreover, the claim about $\mathcal{C}_\rho g_\rho$ is obtained by following the line of reasoning leading to [10, Corollary 5.4] and bearing in mind that the original source is supported inside D. ∎

Since Φ can be written explicitly and the closed and convex set $\mathcal{C}g \subset \mathbb{R}^2$ is determined uniquely by the closed disks enclosing it, Corollary 3.3 can be used to formulate an efficient numerical algorithm for reconstructing the convex source support. This matter is considered in the framework of electric impedance tomography in the following section.

4. An application: Electric impedance tomography. We now turn to the impedance tomography problem of recovering partial information about the unknown conductivity

$$\sigma \in \Sigma := \left\{ \sigma \in L^\infty(D) \,:\, \begin{array}{l} \sigma - 1 \text{ has compact support, and there} \\ \text{exists a constant } \underline{\sigma} > 0 \text{ with } \sigma \geq \underline{\sigma} \text{ a. e.} \end{array} \right\}$$

in (1.1) from one or a few boundary measurements. Even if $\sigma \in \Sigma$ is further restricted to be piecewise continuous, little is known about the identifiability of the support of $\sigma - 1$; see

Isakov [15] for a survey of the corresponding state of the art. On the other hand, this inverse problem has been approached numerically by various authors (cf., e.g., [5, 12, 16, 17, 18, 21]) with quite encouraging results. With the exception of the one in [21], the corresponding numerical algorithms are iterative in nature. However, iterative methods require a repeated solution of varying boundary value problems in the course of the iteration, which may add significantly to the overall cost of these algorithms.

Kwon, Seo, and Yoon [21] have approached the problem from a different viewpoint: They have developed a cheap noniterative method that yields a certain point $P \in D$ which is claimed to be close to the support of $\sigma - 1$. The numerical results shown in [21] indicate that the point P may indeed provide some useful information about the location of $\operatorname{supp}(\sigma - 1)$; a rigorous theoretical analysis for the general setting $\sigma \in \Sigma$, however, is still missing (see [9]). In what follows we will apply the results of the previous sections to come up with an alternative approach for locating this set without much cost.

In doing so we shall restrict our attention to only one fixed but arbitrary boundary current $f \in L^2_\diamond(\partial D)$ and introduce the corresponding reference potential v_0 defined by

$$\Delta v_0 = 0 \quad \text{in } D, \qquad \frac{\partial v_0}{\partial \nu} = f \quad \text{on } \partial D, \qquad \int_{\partial D} v_0 \, \mathrm{d}s = 0\,. \tag{4.1}$$

By subtracting the variational equations for $v, v_0 \in H^1(D)$ (cf., e.g., [6]), it is easy to see that $u = v - v_0$ satisfies

$$\int_D \nabla u \cdot \nabla w \, \mathrm{d}x \;=\; \int_D (1-\sigma)\, \nabla v \cdot \nabla w \, \mathrm{d}x \qquad \text{for all } w \in H^1(D), \tag{4.2}$$

which has a unique solution among $H^1(D)$ elements that integrate to zero over ∂D due to the Lax–Milgram lemma. From (4.2) and Weyl's lemma it follows that the Laplacian of u vanishes away from the support of $\sigma - 1$; moreover, by a standard variational argument, u satisfies the homogeneous Neumann condition on ∂D. As a consequence, $u \in H^1(D)$ is a solution of (1.2) for some source in $H^{-1}(D) \cap \mathcal{E}'_\diamond(D)$ supported in $\operatorname{supp}(\sigma - 1)$ and depending on the unknown conductivity *and* the unknown potential v in (1.1). Note that in real life the needed difference data $u|_{\partial D} = (v - v_0)|_{\partial D}$ can be approximated via electrode measurements [13, 14, 22]. However, in this work we restrict our attention to the ideal situation where the data is given continuously along the boundary; the implementation of our algorithm in the framework of simulated electrode measurements is considered in [8].

To be more specific, we first assume that σ is smooth: In this case partial integration in (4.2) reveals that the source can be written as

$$F \;=\; \nabla \cdot (1-\sigma) \nabla v,$$

which obviously is supported in $\operatorname{supp}(\sigma - 1)$. On the other hand, if σ is piecewise constant, i.e., it equals 1 outside some smooth enough domain Ω, for which $\overline{\Omega} \subset D$, and some other constant within Ω, then (4.2), together with the grounding of the potential on ∂D, is equivalent to the transmission problem

$$\Delta u = 0 \quad \text{in } D \setminus \partial\Omega, \qquad \frac{\partial u}{\partial \nu} = 0 \quad \text{on } \partial D, \qquad \int_{\partial D} u \, \mathrm{d}s = 0,$$
$$\frac{\partial u^+}{\partial \nu} - \frac{\partial u^-}{\partial \nu} = (\sigma^- - 1)\, \frac{\partial v^-}{\partial \nu}, \qquad u^+ - u^- = 0 \quad \text{on } \partial\Omega,$$

where the superscripts + and − correspond to traces taken from within $D \setminus \overline{\Omega}$ and Ω, respectively. This transmission problem can be interpreted as a source problem of the type (1.2) with a distributional source F supported on the boundary of $\operatorname{supp}(\sigma - 1)$.

Recall from the previous sections that the convex source support $\mathcal{C}g$ of some Dirichlet data $g = u|_{\partial D}$, with u given by (1.2), is contained in the convex hull of the support of the source F of (1.2). Moreover, there are compatible sources supported in any arbitrarily small neighborhood of $\mathcal{C}g$. Accordingly, if we let $u = v - v_0$ be the solution of (4.2) and set $g = u|_{\partial D}$, then $\mathcal{C}g$ is a subset of the convex hull of the support of $\sigma - 1$. Of course, we need to solve one forward problem, namely, the Laplace equation (4.1), to obtain $v_0|_{\partial D}$ and thus g; for a more general domain D we also need to solve the diffraction problem (2.2). Still, our method is much cheaper than the iterative methods mentioned above.

Our numerical algorithm for computing $\mathcal{C}g$ is based on Corollary 3.3. It is well known (see again [11]) that all Möbius transformations that map B_ρ onto the unit disk have the form (in complex variables)

$$\Phi(z) = \rho e^{\mathrm{i}c}\, \frac{z - \zeta}{\rho^2 - \overline{\zeta} z}\,, \qquad z \in B_\rho\,, \tag{4.3}$$

where $\zeta \in B_\rho$ is a free parameter and c is a real number. Since our interest is restricted to mappings Φ which take some given closed disk $B \subset B_\rho$ onto a disk $\overline{B}_R$ centered at the origin as in Figure 2, the parameter c is irrelevant for our purposes and will be set to zero in what follows. We emphasize that Φ maps ζ onto the origin, but *does not* map a disk centered at ζ onto a disk centered at the origin—unless $\zeta = 0$. However, any closed disk $B \subset B_\rho$ can be mapped by some transformation Φ of this form, with $\zeta \in B$ and $c = 0$, onto some concentric disk $\overline{B}_R$. Moreover, R and ζ are uniquely determined this way. As a consequence, we can test all disks in B_ρ by varying the parameter $\zeta \in B_\rho$ and $0 < R < 1$ and checking (3.2) for convergence.

This test for convergence can be implemented using an idea from [4]. With increasing frequency the Fourier coefficients $\alpha_j(\Phi)$ of $g_\rho \circ \Phi^{-1}$ typically show a geometric decay. It is therefore natural to approximate

$$\log |\alpha_j(\Phi)| \;\approx\; m|j| + b\,, \tag{4.4}$$

e.g., by a standard linear regression analysis, and to assume that the series (3.2) converges whenever $R > e^m$. We vary $\zeta \in Z$ for some finite subset $Z \subset B_\rho$, and accordingly $\Phi = \Phi_\zeta$ from (4.3) with $c = 0$, and define the associated radii $R_\zeta = e^m$ with $m = m_\zeta$ of (4.4). Based on these computations we find

$$\mathcal{C}g \;\approx\; \bigcap_{\zeta \in Z} \Phi_\zeta^{-1}(B_{R_\zeta})\,. \tag{4.5}$$

Note that, as ρ increases, this approximation gets, in principle, better because larger disks may enter the intersection in (4.5), but at the same time more grid points are needed to obtain a proper covering of B_ρ. Even more importantly, the relation (3.1) shows that the small details in g_ρ vanish extremely rapidly as ρ gets larger, and thus increasing ρ makes the algorithm more susceptible to (even numerical) noise. As a consequence, there is a trade-off

between the theoretical optimality and the stability of the algorithm. Our numerical tests indicate that the reconstructions usually deteriorate if $\rho > 1.5$; in the examples presented below we use $\rho = 1.4$.

For our numerical experiments we solved the forward problem with the boundary element code from [4] using $N = 768$ equidistant grid points for the Dirichlet boundary value $g = u|_{\partial D}$. We compute the "propagated data" g_ρ on ∂B_ρ by using the relation (3.1) and then approximate the Fourier coefficients of $g_\rho \circ \Phi_\rho^{-1}$ by

$$\begin{aligned}\alpha_j(\Phi) &= \frac{1}{2\pi}\int_{-\pi}^{\pi} g_\rho\big(\theta(s)\big)\, e^{-\mathrm{i}js}\,\mathrm{d}s = \frac{1}{2\pi}\int_{-\pi}^{\pi} g_\rho(\theta)\, e^{-\mathrm{i}js(\theta)} s'(\theta)\,\mathrm{d}\theta \\ &\approx \frac{1}{N}\sum_{k=1}^{N} g_{\rho,k}\, e^{-\mathrm{i}js(\theta_k)} s'(\theta_k)\,,\end{aligned}$$

where $g_{\rho,k} = g_\rho(\theta_k)$ and $\theta_k = kh$ with $h = 2\pi/N$. The function $s = s(\theta)$ parameterizes the boundary map corresponding to Φ; i.e., for $\zeta = re^{\mathrm{i}\varphi} \in Z$ and $z = \rho e^{\mathrm{i}\theta}$ with $-\pi < \theta \le \pi$ we have

$$s(\theta) = \varphi + 2\arctan\left(\frac{\rho + r}{\rho - r}\tan\left(\frac{\theta - \varphi}{2}\right)\right)$$

(up to multiples of 2π) with derivative

$$s'(\theta) = \frac{\rho^2 - r^2}{\rho^2 - 2\rho r\cos(\theta - \varphi) + r^2}\,.$$

Note that $g_\rho \circ \Phi_\rho^{-1}$ is no longer given on an equidistant mesh, and the quality of the above quadrature rule for approximating $\alpha_j(\Phi)$ thus deteriorates when j becomes large or when ζ approaches ∂B_ρ. We avoid this by restricting $Z \subset B_{\rho_0}$ for some number $\rho_0 < \rho$. Our experience suggests that ρ_0 should be less than 0.7ρ, say. It has to be emphasized, though, that ρ_0 should also be big enough to include some ζ between ∂B_ρ and the center of mass of any of the components of the inhomogeneity, since only those values of ζ provide any information about the inclusion boundary in the "shadow region." Furthermore, we have observed that parameters ζ near the origin rarely contribute significantly to the overall intersection (4.5). Bearing these considerations in mind, we choose Z to be an equidistant grid consisting of 64 points on a circle of radius $r_0 = 4/7\rho$, i.e., $r_0 = 0.8$ in our setting.

Concerning the stability of the algorithm, it is important to note that the number of Fourier terms that stick out of the inherent noise in the data depends on (besides the amount of noise, of course) their decay rate, i.e., on R_ζ. Therefore, the number of Fourier coefficients to be considered reliable for (4.4) has to be chosen adaptively and separately for each point $\zeta \in Z$. We also deleted from Z those parameters ζ for which the number of reliable Fourier coefficients dropped below five.

5. Numerical results.

Now we present three numerical examples in the framework of EIT. Our first test examines the effect that the choice of the input current has on the reconstruction. In the second experiment, we test how the algorithm works with an inhomogeneity that has two disjoint components. Finally, the third example considers noisy measurement. In all three

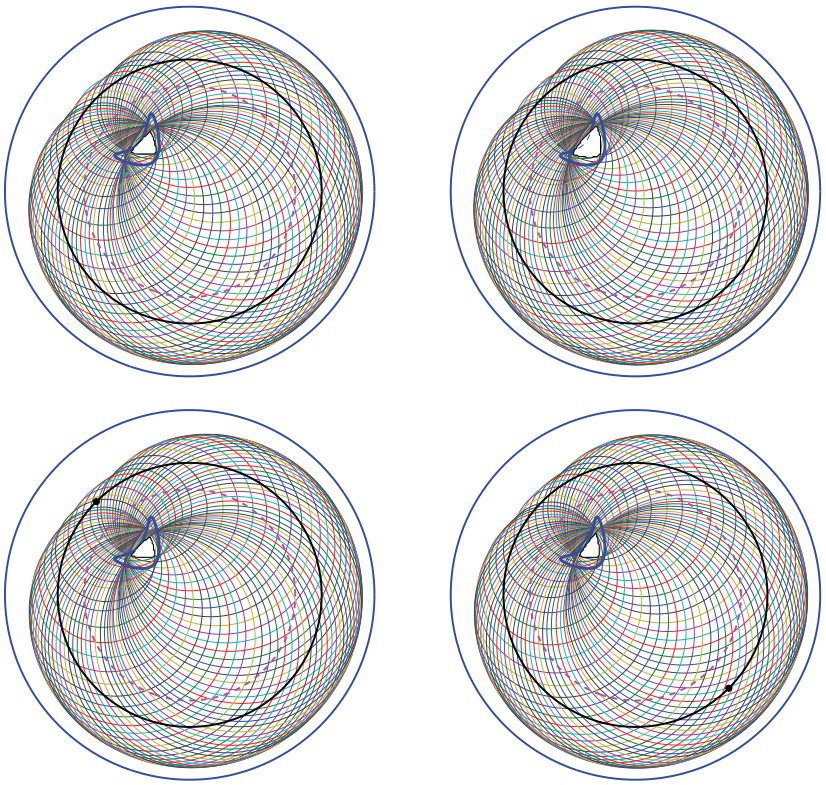

Figure 3. *Reconstructions for different current patterns (see text).*

experiments we consider piecewise constant conductivities; the conductivity of the inclusions is 0.5 if not stated otherwise.

In the first example, we try to detect one kite-shaped inclusion. For this test we have used four different current patterns to compute the reconstructions shown in Figure 3: The two reconstructions in the top row correspond to trigonometric input currents, $f(\theta) = \sin\theta$ on the left and $f(\theta) = \cos(5\,\theta)$ on the right, respectively. The two reconstructions in the second row correspond to more localized currents, computed from the partial sum of the first 64 terms of a trigonometric series approximating a dipole at the boundary of the disk. These currents are meant to simulate measurements taken with two electrodes that are attached close to each other on ∂D. The location of the approximate dipole is marked by a big black spot in each of the two plots: For the left-hand plot the dipole is located close to the inclusion; the right-hand plot corresponds to a dipole sitting on the opposite side of the circle. Here and in the subsequent reconstructions, the outer thick solid circle depicts ∂B_ρ, the inner thick solid circle is ∂D, and the dashed curve marks the circle on which the ζ parameters lie. Furthermore, the many thin circles depict the disks whose intersection—the white area in the interior of the kite—gives an approximation of $\mathcal{C}g$.

As Figure 3 demonstrates, our algorithm locates the inclusion with all four current patterns. In fact, the somewhat counterintuitive conclusion is that the reconstructions are pretty much independent of the used boundary current—at least for exact data. However, as the

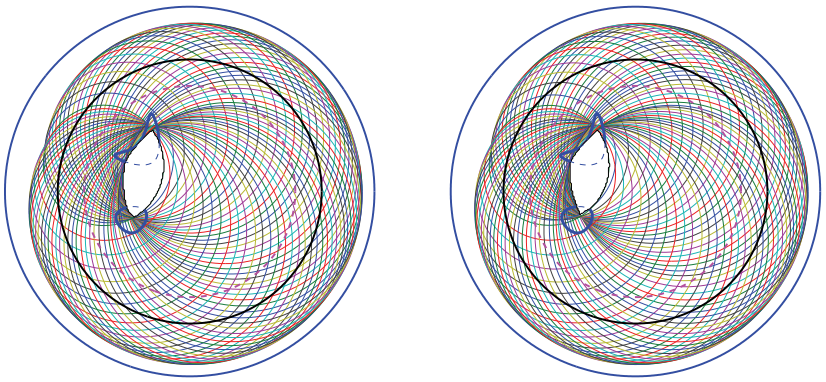

Figure 4. *Reconstructions of two disjoint inclusions. Left: The conductivity of the lower inclusion is* 0.5. *Right: The conductivity of the lower inclusion is* 0.9 *(see text).*

magnitude of the measured signal typically decreases rapidly for increasing Fourier modes in the boundary current, the signal-to-noise ratio is usually much better for low-frequency boundary currents. On the other hand, our experience suggests that the relative size of the convex source support—or at least that of the reconstruction provided by our algorithm—depends significantly on the inhomogeneity in question: the more complicated the inclusion, the larger the convex source support compared to the actual inclusion.

In our second example, we examine how the reconstruction of the first experiment corresponding to the current $f(\theta) = \sin\theta$ is affected if a second inclusion is introduced inside D. We let the conductivity of the new inhomogeneity take two different values: 0.5 and 0.9. As Figure 4 illustrates, the convex source support seems to intersect both inclusions with both conductivity levels. In fact, the conductivity of the lower inclusion does not seem to have much effect on the reconstruction when dealing with noiseless data. It is probable, however, that the reconstructions provided by our algorithm are somewhat smoother and larger than the actual convex source supports since we cannot intersect with arbitrarily large disks (cf. [10] for a similar conclusion).

In our final example, we investigate the robustness of our algorithm with respect to the amount of noise in the data. This time around, we aim at locating a roundish inclusion using once again the boundary current $f(\theta) = \sin\theta$. Let $\overline{g} \in \mathbb{R}^{768}$ denote the values of g at the grid points on ∂D. We simulate noisy measurements by replacing the exact point values $\overline{g}$ in our algorithm by

$$\overline{g}_{n,\delta} = \overline{g} + \frac{\delta}{100}\,\frac{n}{|n|}|\overline{g}|,$$

where $|\cdot|$ denotes the Euclidean norm, the components of $n \in \mathbb{R}^{768}$ are realizations of a normally distributed random variable with zero mean and variance 1, and δ is, loosely speaking, the percentage of noise in the data.

In Figure 5 the first row corresponds to the noise level $\delta = 0.1$ and the second row to $\delta = 1$. The left-hand column shows the reconstruction provided by our algorithm, i.e., the empty set in both cases. Fortunately, with both noise levels the area where almost all test circles intersect clearly points out the approximate location of the inclusion. The lack of

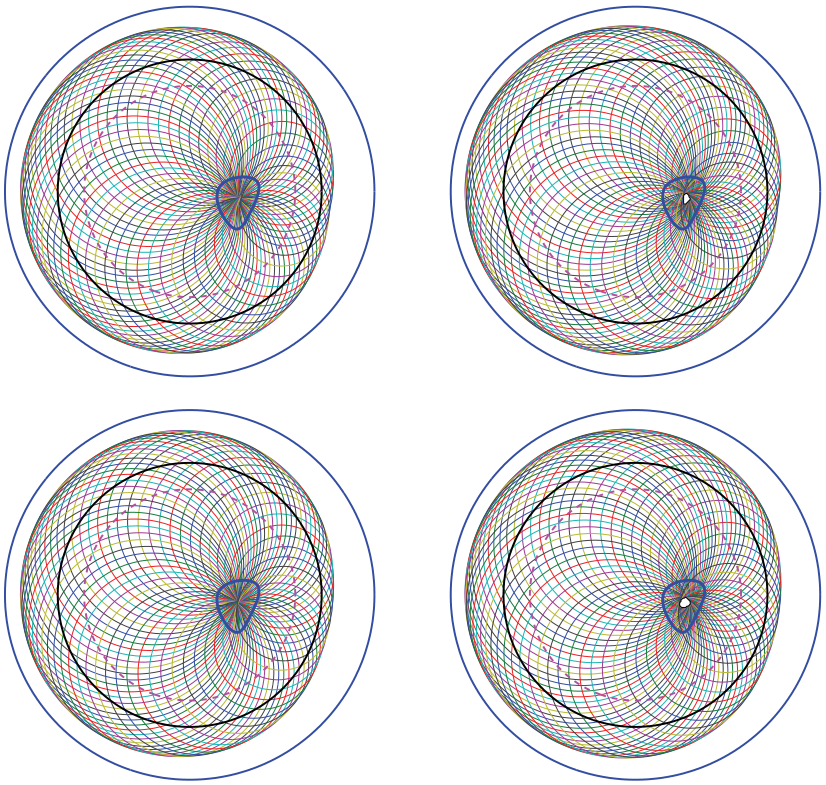

Figure 5. *Reconstructions with noisy data. Top:* 0.1% *of noise. Bottom:* 1% *of noise (see text).*

reconstructions has two potential explanations: First, in many instances the initial decay rate of the Fourier coefficients $\alpha_j(\Phi)$ is somewhat more pronounced than in the long run. When the measurement is noisy, the number of reliable Fourier coefficients is low (in this example, for $\delta = 0.1$ around ten, and for $\delta = 1$ six), which may thus lead to too small test disks and cause the loss of reconstruction. Second, the measurement noise may also result in deceptively small outliers in the family of test disks; one such outlier may be enough to make the whole reconstruction disappear.

In the right-hand column of Figure 5, we have addressed the problem by replacing the optimal radii $\{R_\zeta\}_{\zeta\in Z}$ in (4.5) by the slightly larger $\{R_\zeta + \epsilon\}_{\zeta\in Z}$, where ϵ is chosen to be 0.02. With both noise levels this results in the appearance of a small intersection of the corresponding test disks at the middle of the actual inclusion. Since there is no way of defining the "correct value" of the auxiliary parameter ϵ, this approach can point out only the location of the convex source support, not its shape or size.

6. Concluding remarks. In our numerical examples we have restricted our attention to the case where only one pair of Cauchy data is available for impedance tomography. If more than one pair of data is given, one can of course combine the corresponding reconstructions, as each of them should lie inside the convex hull of $\operatorname{supp}(\sigma - 1)$; cf. section 4. However, our numerical results did not really benefit from such a modification, as all individual reconstructions were pretty much alike; cf. Figure 3.

REFERENCES

[1] K. Astala and L. Päivärinta, *Calderón's inverse conductivity problem in the plane*, Ann. of Math. (2), 163 (2006), pp. 265–299.

[2] L. Borcea, *Electrical impedance tomography*, Inverse Problems, 18 (2002), pp. R99–R136.

[3] L. Borcea, *Addendum to: "Electrical impedance tomography"* [Inverse Problems, 18 (2002), R99–R136], Inverse Problems, 19 (2003), pp. 997–998.

[4] M. Brühl and M. Hanke, *Numerical implementation of two noniterative methods for locating inclusions by impedance tomography*, Inverse Problems, 16 (2000), pp. 1029–1042.

[5] K. Bryan, *Numerical recovery of certain discontinuous electrical conductivities*, Inverse Problems, 7 (1991), pp. 827–840.

[6] R. Dautray and J.-L. Lions, *Mathematical Analysis and Numerical Methods for Science and Technology*, Vol. 2, Springer, Berlin, 1988.

[7] H. Haddar, S. Kusiak, and J. Sylvester, *The convex back-scattering support*, SIAM J. Appl. Math., 66 (2005), pp. 591–615.

[8] H. Hakula and N. Hyvönen, *Two noniterative algorithms for locating inclusions using one electrode measurement of electric impedance tomography*, Inverse Problems, 24 (2008), 055018.

[9] M. Hanke, *On real-time algorithms for the location search of discontinuous conductivities with one measurement*, Inverse Problems, 24 (2008), 045005.

[10] M. Hanke, N. Hyvönen, M. Lehn, and S. Reusswig, *Source supports in electrostatics*, BIT, 48 (2008), pp. 245–264.

[11] P. Henrici, *Applied and Computational Complex Analysis*, Vol. 1, Wiley, New York, 1974.

[12] F. Hettlich and W. Rundell, *The determination of a discontinuity in a conductivity from a single boundary measurement*, Inverse Problems, 14 (1998), pp. 67–82.

[13] N. Hyvönen, *Complete electrode model of electrical impedance tomography: Approximation properties and characterization of inclusions*, SIAM J. Appl. Math., 64 (2004), pp. 902–931.

[14] N. Hyvönen, *Approximating idealized boundary data of electric impedance tomography by electrode measurements*, submitted.

[15] V. Isakov, *Inverse Problems for Partial Differential Equations*, 2nd ed., Springer, Berlin, 2006.

[16] K. Ito, K. Kunisch, and Z. Li, *Level-set function approach to an inverse interface problem*, Inverse Problems, 17 (2001), pp. 1225–1242.

[17] H. Kang, J. K. Seo, and D. Sheen, *Numerical identification of discontinuous conductivity coefficients*, Inverse Problems, 13 (1997), pp. 113–123.

[18] R. Kress and W. Rundell, *Nonlinear integral equations and the iterative solution for an inverse boundary value problem*, Inverse Problems, 21 (2005), pp. 1207–1223.

[19] S. Kusiak and J. Sylvester, *The scattering support*, Comm. Pure Appl. Math., 56 (2003), pp. 1525–1548.

[20] S. Kusiak and J. Sylvester, *The convex scattering support in a background medium*, SIAM J. Math. Anal., 36 (2005), pp. 1142–1158.

[21] O. Kwon, J. K. Seo, and J-R. Yoon, *A real-time algorithm for the location search of discontinuous conductivities with one measurement*, Comm. Pure Appl. Math., 55 (2002), pp. 1–29.

[22] A. Lechleiter, N. Hyvönen, and H. Hakula, *The factorization method applied to the complete electrode model of impedance tomography*, SIAM J. Appl. Math., 68 (2008), pp. 1097-1121.

[23] A. I. Nachman, *Global uniqueness for a two-dimensional inverse boundary value problem*, Ann. of Math. (2), 143 (1996), pp. 71–96.

[24] R. Potthast, J. Sylvester, and S. Kusiak, *A 'range test' for determining scatterers with unknown physical properties*, Inverse Problems, 19 (2003), pp. 533–547.

[25] J. Sylvester, *Notions of support for far fields*, Inverse Problems, 22 (2006), pp. 1273–1288.

[26] J. Sylvester and J. Kelly, *A scattering support for broadband sparse far field measurements*, Inverse Problems, 21 (2005), pp. 759–771.

[27] J. Sylvester and G. Uhlmann, *A global uniqueness theorem for an inverse boundary value problem*, Ann. of Math. (2), 125 (1987), pp. 153–169.